# 3D electrical conductivity imaging of Halema‘uma‘u lava lake (Kīlauea volcano)

Lydie Gailler, Jim Kauahikaua, Jean-François Lénat, André Revil, Marceau Gresse, Abdellahi Soueid Ahmed, Nicolas Cluzel, Geeth Manthilake, Lucia Gurioli, Tim Johnson, et al.

Journal of Volcanology and Geothermal Research 381 (2019) 185–192

Contents lists available at ScienceDirect

Journal of Volcanology and Geothermal Research

journal homepage: www.elsevier.com/locate/jvolgeores

# 3D electrical conductivity imaging of Halema'uma'u lava lake (Kīlauea volcano)

Lydie Gailler [a,*], Jim Kauahikaua [b], Jean-François Lénat [a], André Revil [c], Marceau Gresse [d], Abdellahi Soueid Ahmed [c], Nicolas Cluzel [a], Geeth Manthilake [a], Lucia Gurioli [a], Tim Johnson [e], Anthony Finizola [f], Eric Delcher [f]

[a] Laboratoire Magmas et Volcans, Université Clermont Auvergne, CNRS, IRD, OPGC, Campus Universitaire des Cézeaux, 6 Avenue Blaise Pascal, 63178 AUBIERE Cedex, France
[b] U.S.G.S. Hawaiian Volcano Observatory, PO Box 51, 1 Crater Rim Road, Hawai'i National Park, HI 96718, United States of America
[c] Univ. Grenoble Alpes, Univ. Savoie Mont Blanc, CNRS, IRD, IFSTTAR, ISTerre, 38000 Grenoble, France
[d] Earthquake Research Institute, University of Tokyo, Tokyo, Japan
[e] Pacific Northwest National Laboratory, Richland, WA 99352, United States of America
[f] Laboratoire GéoSciences Réunion, Université de la Réunion, IPGP, Sorbonne Paris-Cité, CNRS UMR 7154, 15 Avenue René Cassin, CS 92003, 97744 Saint-Denis, La Réunion, France

ARTICLE INFO

*Article history:*
Received 8 February 2019
Received in revised form 5 June 2019
Accepted 7 June 2019
Available online 10 June 2019

ABSTRACT

Before the 2018 collapse of the summit of Kīlauea volcano, a ca. 200 m in diameter lava lake inside of Halema'uma'u crater was embedded in a very active hydrothermal system. In 2015, we carried out an electrical conductivity survey and the data were inverted in 3D. The lack of conductivity contrast precludes distinguishing the lava column from the surrounding hydrothermal zones. Laboratory measurements on samples from the lava lake show that the conductivity of magma is significantly lower than that of hydrothermal zones but the high vesicularity of the upper part of the lava lake may decrease its macroscopic conductivity. Based on the 3D conductivity model, we distinguish at least two types of hydrothermal circulations: 1) one guided by the collapse faults of Halema'uma'u crater and by the magmatic column of the lava lake, and 2) another guided by previous caldera faults and fractures related to intrusions. We observe that the location of the faults formed during the 2018 collapse of the summit was greatly influenced by the hydrothermally altered zones.



## 1. Introduction

The detection of magma at depth and the quantification of its macroscopic properties (melt fraction, volume and magma distribution) are among the most important challenges in volcanology. Geophysical methods such as seismology, deformation, magnetic and electrical resistivity methods may be used for that purpose. Because the velocity and attenuation of elastic waves depend on the mechanical properties of the medium, seismic methods have the potential to detect the presence of magma (Murase and McBirney, 1973). With these methods, the presence of melts has been inferred in various environments from oceanic ridges to the upper mantle of subduction zones and volcanoes (see a review in Lees, 2007). However, the wavelengths of the seismic waves used in these studies are sometimes too large (several tens of kilometers; e.g., Pritchard and Gregg, 2016) to detect small magmatic bodies (a few tens of meters) especially at shallow depths. Using deformation techniques, inflation/deflation cycles of volcanic areas are often interpreted as pressurization/depressurization of magma bodies. Modelling allows estimating the size, depth and geometry of these bodies, but ambiguity remains on the nature of the fluids, because hydrothermal fluids may also generate comparable deformation (e.g., Gambino and Guglielmino, 2008; Hurwitz et al., 2007). Magnetic methods also have potential for detecting and imaging magma bodies at depth, because, above the Curie temperature (580 °C), the magma is paramagnetic. Thus, in high temperature zones the magnetic signal vanishes. This phenomenon has been used to map the Curie isotherm at great depth at the scale of a large area (e.g. Blakely, 1988; Tanaka et al., 1999: ~5800 × $10^3$ $km^2$) or at shallow depth in smaller areas (e.g. Gailler et al., 2016, 2017: ~810 × $10^3$ $km^2$). Electrical measurements are well suited for imaging the interior of active volcanoes, because the resistivity of volcanic rocks spans several orders of magnitude (Lénat, 1995) and because magmas have the lowest resistivity values in volcanic environment ranging from about 20 to <1 Ω.m (see Lénat, 1995 and references therein). However, hydrothermally altered rocks (e.g. zeolites, clay and sulfate minerals) and active hydrothermal systems (hot mineralized fluids, altered rocks) may show resistivity values only slightly larger than that of melts (Legaz et al., 2009; Murase and McBirney, 1973; Revil et al., 2008, 2004, 2002; Revil and Jardani, 2010). Studying large magma bodies remains challenging

* Corresponding author.
*E-mail address:* l.gailler@opgc.univ-bpclermont.fr (L. Gailler).

https://doi.org/10.1016/j.jvolgeores.2019.06.001
0377-0273/

because of the ambiguities in the interpretation of geophysical data for the detection of magma. Active lava lakes are probably the best geological structures with which to test the ability of geophysical methods for detecting magma. There are presently a limited number of active lava lakes: Erta Ale (Ethiopia), Ambrym (Vanuatu), Mount Erebus (Ross Island, Antarctica), Nyiragongo (Democratic Republic of the Congo), Masaya (Nicaragua) and Kīlauea (Hawai'i) until 2018. Among those, Kīlauea's was the most suitable site for experiments at close range in terms of accessibility, dimension, depth of the magma column and collection of fresh samples.

In 2015, we carried out an electrical resistivity experiment around Halema'uma'u lava lake using multi-electrodes arrays and direct current to probe the lava lake and the extent of its surrounding hydrothermal system. To our knowledge, this is the first time that such measurements of a large body of magma were made at close range. This survey also offers a unique detailed dataset to study the Halema'uma'u lava lake before it receded in May 2018.

## 2. Geological context

Kīlauea volcano (Hawai'i) remains undoubtedly an iconic edifice with a complex history of effusive and explosive cycles (Swanson et al., 2014). At least two cycles of explosive and effusive eruptions have occurred in the last 2200 years following collapse of the Powers caldera ca. 200 BCE (Holcomb, 1987; Powers, 1948), and the modern caldera ca. 1500 CE (Swanson et al., 2012). A major feature of the present summit caldera is Halema'uma'u crater (Fig. 1). This crater has hosted several lava lakes, with the latest one, informally called Halema'uma'u Overlook Crater, first appearing in March 2008 following a small explosive eruption near the SE rim of Halema'uma'u crater (Orr et al., 2013). Its surface diameter progressively increased to 200 m when it disappeared in 2018 on May 10 during the caldera collapse. A large-scale subsidence of the caldera floor around Halema'uma'u began in mid-May and lasted until early August (Neal et al., 2019). The lava lake had been closely monitored by the Hawaiian Volcano Observatory (HVO) for hazards reasons and for research. Several recent projects have increased our understanding of how the lava lake worked and how it interacted with Kīlauea's system as a whole: seismology (Chouet and Dawson, 2013; Patrick et al., 2011), gravity (Carbone and Poland, 2012; Poland and Carbone, 2016), thermal imaging (Patrick et al., 2015; Patrick et al., 2016), deformation (Richter et al., 2013), as well as quantification and analysis of eruptive products (Eychenne et al., 2015; Swanson et al., 2009).

### 2.1. The resistivity experiment

Electrical Resistivity Tomography (ERT) field mapping consists of sequential quadripole resistivity measurements along profiles: an electrical current is injected into the ground between two current electrodes A and B and the resulting electrical potential distribution is sampled between two voltage electrodes M and N. An apparent resistivity (in ohm.m) can be determined using the electrode geometry, the injected current and the measured difference of electrical potential.

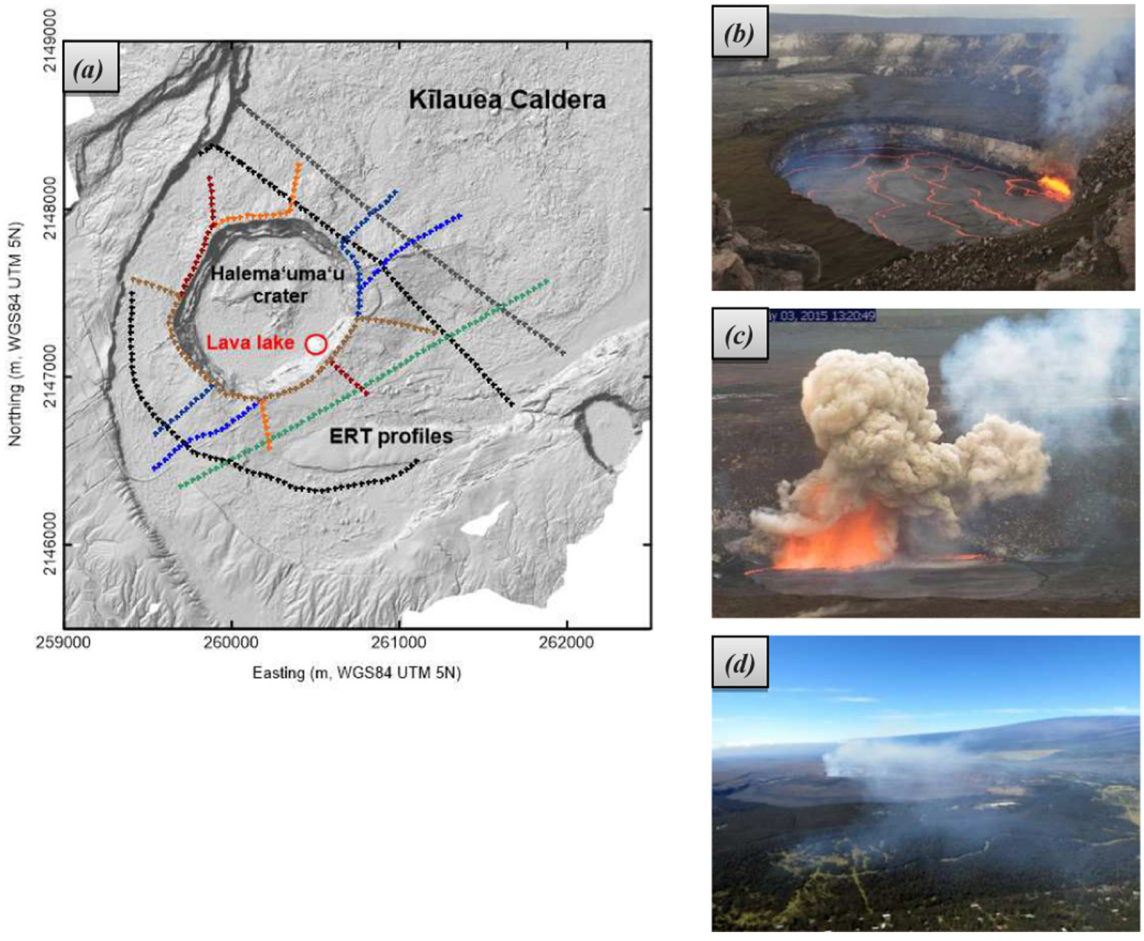


**Fig. 1.** The Lava lake of Kīlauea Volcano. a) Location of the ERT profiles around the lava lake in Halema'uma'u crater in the summit caldera of Kīlauea Volcano; base map is a lidar image with 1 m resolution. Location of the active lava lake is shown. b) Weak spattering that produces Pele's hair, Pele's tears, and other glassy pyroclasts. c) Explosive event triggered by a rock fall into the lava lake and producing highly vesicular spatter. d) Gas plume during typical lava lake activity. Photos obtained from https://volcanoes.usgs.gov/volcanoes/Kīlauea/archive/multimedia/index.shtml.

Electrical resistivity measurements were performed in November 2015 around Halema'uma'u lava lake along ten profiles each 2.5 km in length, using Wenner electrode configuration (best for the detection of horizontal contacts) with a set of 64 stainless steel electrodes spaced at 40 m intervals along a 2 km profile. A curvilinear geometry of the electrode arrays around the crater (Fig. 1a) was especially tailored to generate current-lines passing through the lava lake along 7 profiles (an example is provided in Fig. C1 in Supplementary data C). 4945 resistivity measurements were acquired and filtered to remove the low signal-to-noise ratio or spurious data. A 3D ERT (E4D) code from Johnson et al. (2010) was used to derive the conductivity model. A complete description of the parallel inversion algorithm is given in Johnson et al. (2010) (see Supplementary data C for more information).

In order to check the detectability of the conductive magma column, forward theoretical 3D models that depict a conductivity pattern similar to the one expected in the Halema'uma'u area were calculated using E4D software (see Fig. A1 in Supplementary data A). Three forward models were developed and synthetic data generated from these were inverted to test the effect of 1) a highly conductive lava lake, 2) a large conductive hydrothermal system and 3) the combination of both conductive bodies embedded in a highly resistive environment (mostly unsaturated lava flows) as a starting model. Forward modelling was performed to mimic as closely as possible the field conditions with the same configuration as used for the 3D inversion (mesh, number of elements; see Supplementary data C for additional information). We note that very small structures such as the magma column are difficult to recover even with very low conductive values (i.e. a few S/m). Our forward tests show the primary contribution to the conductivity models is from the hydrothermal system with only a minor effect that could be attributed to the lava lake.

### 2.2. Microscopic physical properties of the lava lake

Inferring the internal physical state of the lava lake is ~~also~~ fundamental to quantify the in situ conductivity and verify the reliability of the 3D conductivity model. The magma of the lake may be sampled with ejecta emitted during explosive events and Pele's hairs continuously formed by spattering at the surface of the lake. Such samples enable us to carry out laboratory measurements to quantify the electrical conductivity of the magma and the density-derived vesicularity of the pyroclasts.

Electrical conductivity measurements were performed on three Hawaiian basaltic glass samples (Fig. C2 in Supplementary data C) using an impedance gain-phase analyzer in the $10^1$–$10^6$ Hz frequency range. The high-pressure and high temperature experiments were performed in a multi-anvil apparatus at Laboratoire Magmas et Volcans (LMV). The samples were chosen to represent different degrees of degassing and variable amounts of vesicularity. The low confining pressure (500 MPa) was chosen to preserve the sample vesicles during the initial hydrostatic compression of the high-pressure assembly. The conductivity of basaltic glass increases continuously with increasing temperature from 200 to 1200 °C as shown on Fig. 2a. Before melting all three samples show similar conductivity values around $10^{-2}$ S/m. Upon melting, at around 1100 °C, the conductivity of samples discontinuously increased by two orders magnitude to ~1 S/m at 1200 °C.

For vesicularity measurements, several specimens of quenched ejecta (from 5 to 10 cm in size) produced during explosive events of the Kīlauea lava lake activity, as well as Pele's hair were sampled (Fig. C2 in Supplementary data C). Density measurements of the samples were performed using a pycnometer (Micromeritics Geopyc 1360 envelope density analyzer, at Laboratoire Magmas et Volcans (LMV) for samples smaller than 5 cm in diameter. The water immersion technique described in Houghton and Wilson (1989), which is based on Archimedes' principle, was instead used for samples bigger than 5 cm in diameter. Measurement for both these approaches was determined to a precision of $\pm 10^{-2}$. The vesicularity was obtained using the dense rock equivalent (DRE) measured with the Accupyc 1340 Helium Pycnometer on the same powdered samples. The same pycnometer was used to measure the connected porosity for each clast using the method described in Formenti and Druitt (2003). We calculated the pore connectivity by dividing the connected porosity by the total porosity. For

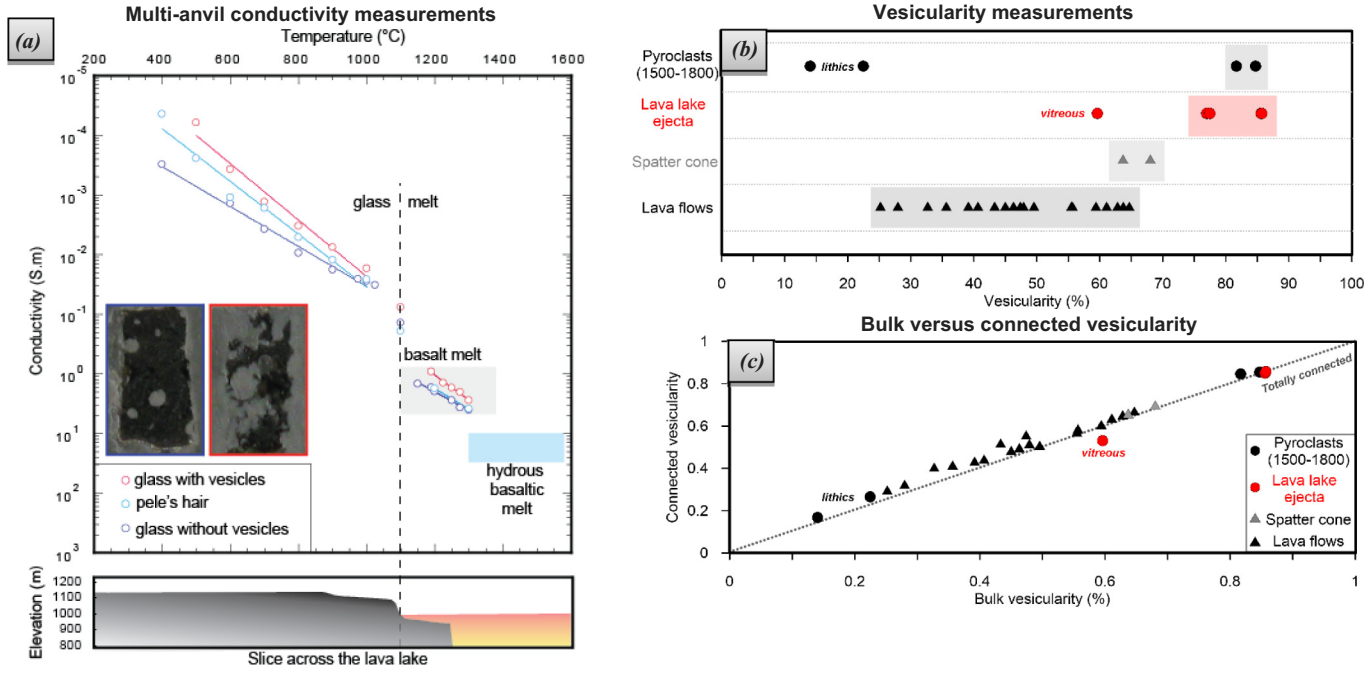


**Fig. 2.** Measurements on lava lake samples: a) Variation of the conductivity measurements with temperature for each sample: glassy and vesicular parts of pyroclasts shown as assemblages before the experiment, Pele's hair crushed before melting. The blue shaded area indicates electrical resistivity of hydrous basalt at high temperature (Ni et al., 2011). b) Comparison of the vesicularity (%) of the lava lake ejecta with several types of samples in the environment of the crater. c) Diagram of bulk vesicularity versus connected vesicularity showing that all the bubbles are connected. (For interpretation of the references to colour in this figure legend, the reader is referred to the web version of this article.)

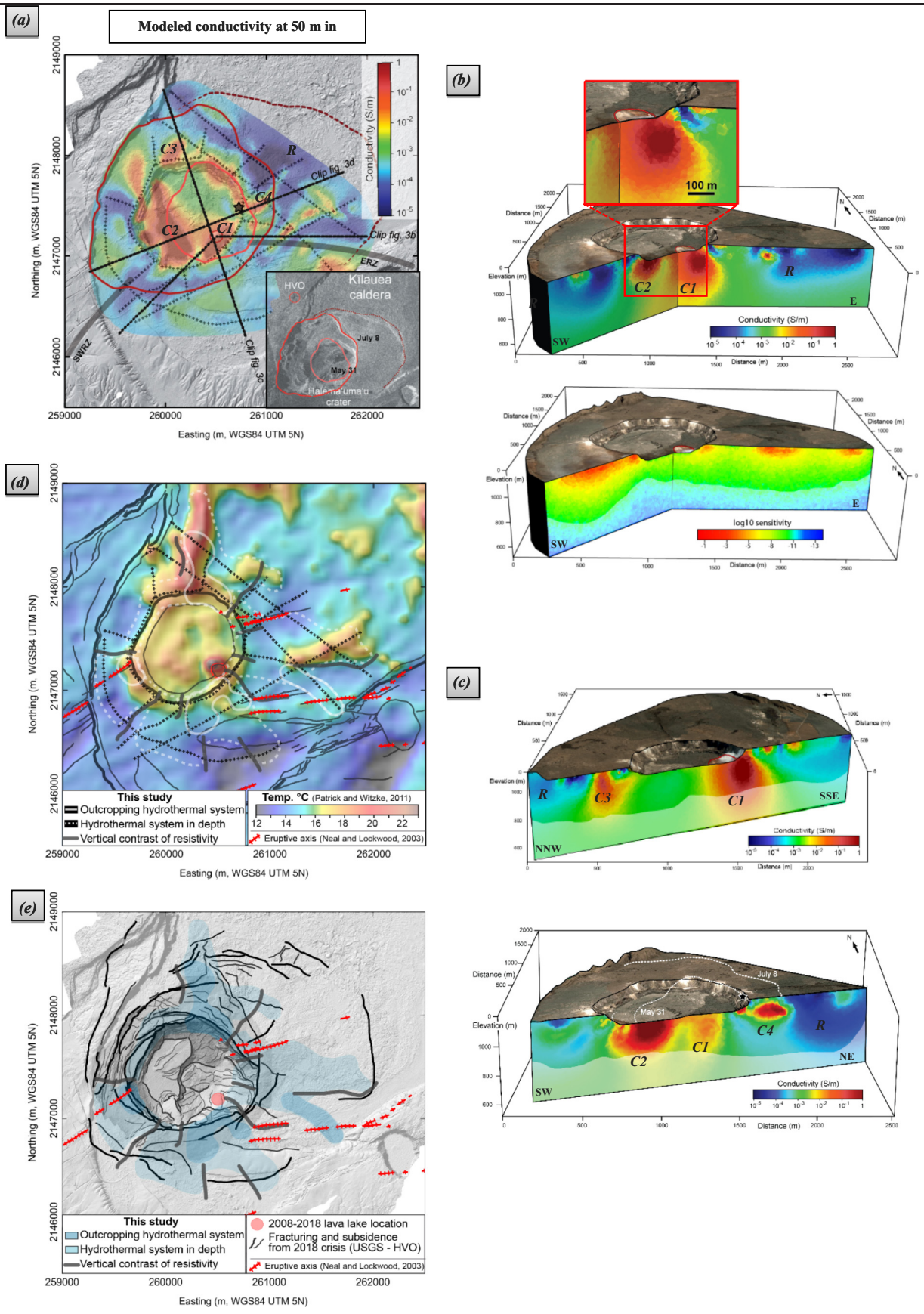
(a)
Modeled conductivity at 50 m in
Conductivity (S/m)
C1
C2
C3
C4
R
Clip fig. 3d
Clip fig. 3b
Clip fig. 3c
ERZ
SWRZ
HVO
Kilauea caldera
July 8
May 31
Halema'uma'u crater
Northing (m, WGS84 UTM 5N)
Easting (m, WGS84 UTM 5N)
(b)
100 m
Conductivity (S/m)
log10 sensitivity
SW
E
(c)
NNW
SSE
(d)
This study
Outcropping hydrothermal system
Hydrothermal system in depth
Vertical contrast of resistivity
Temp. °C (Patrick and Witzke, 2011)
Eruptive axis (Neal and Lockwood, 2003)
(e)
2008-2018 lava lake location
Fracturing and subsidence from 2018 crisis (USGS - HVO)
NE

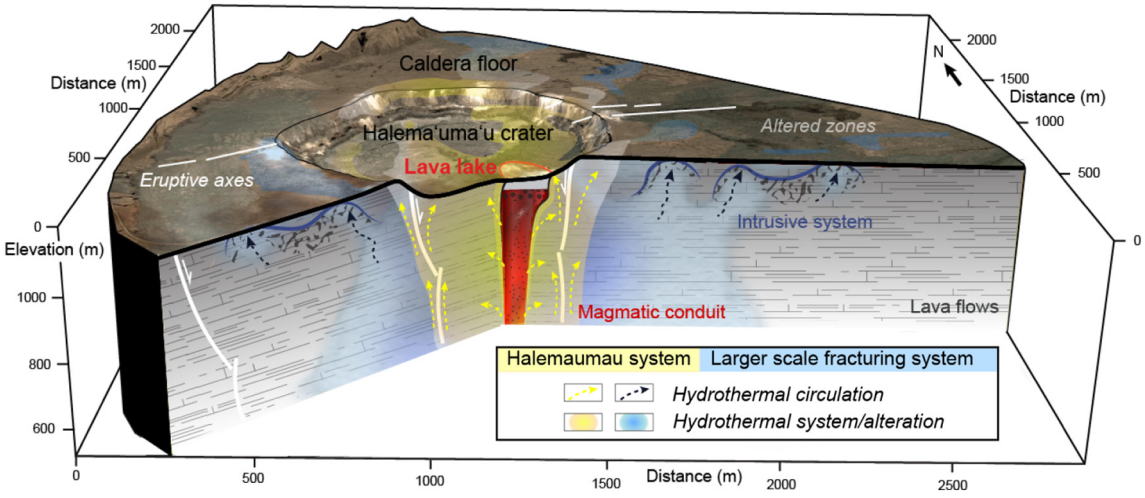


**Fig. 4.** Synthetic interpretative scheme, derived from our 3D conductivity model combined with geological information such as fracturing (Roche et al., 2000) and zones of alteration based on thermal anomaly map (Patrick and Witzke, 2011).

vesicularity and density measurements, various types of samples were also analysed for petrophysical comparison (Fig. C2 in Supplementary data C).

Our laboratory-based electrical conductivity measurements of Pele's hairs and pyroclasts (Fig. 2a) indicate conductivity as high as 1 S/m at temperatures above their melting temperature (~1150 °C). The density-derived vesicularity values of the pyroclasts are >75 vol% (Fig. 2b), in agreement with the low density of the upper part of the lava lake suggested by gravity measurements (Carbone et al., 2013; Poland and Carbone, 2016). Because the vesicles of the pyroclasts are totally connected (Fig. 2c), the conductivity values of the melted samples should be representative of the lava lake. Calculations with Sigmelts (Pommier and Le-Trong, 2011) show that for a 1 S/m magma containing 80% of resistive spherical gas vesicles, the bulk conductivity of magma plus vesicles decreases to about 1.4 $10^{-1}$ S/m.

Considering that in a natural system, gas bubbles concentrate in the upper part of the magma column, the conductivity derived from the measurements on the lava lake samples may be considered as a good estimate of that of the upper part of the magma column, as confirmed by the in-situ measurements performed at Kīlauea Iki lava lake (Smith et al., 1977) and lava flow (Bartel et al., 1983). Such low conductivity values are commonly associated with low density materials in agreement with the recent estimated densities of the lava lake (Carbone et al., 2013). Joint analysis of gravity and lava level time series data (Poland and Carbone, 2016) recorded over a large period (2011–2015) have shown a low average density (1000–1500 kg $m^{-3}$) of the lava within the upper tens to hundreds of meters. As a comparison, density of vesicle-free lava has been estimated in the first ten of meters for other Hawaiian lava lakes samples, giving melt fraction density of about 2740 kg $m^{-3}$ for ʻAlae lava lake and 2730 to 2750 kg $m^{-3}$ for Makaopuhi lava lake (Peck, 1978) at temperatures higher than 1100 °C. Accordingly, the very low-density values estimated at the scale of Halemaʻumaʻu lava lake can be connected to high vesicularity at least in the upper magma column in the summit vent.

## 3. Results: 3D conductivity model of a complex volcanic zone

A priori knowledge of the geometry of the magma column would be an important constraint for modelling. It is difficult to establish, but some variations of the lake level have provided insights onto the shape of the magma column at depth. In March 2011, the lake dropped >210 m, allowing the mapping of the upper conduit (Orr et al., 2013). The diameter at the surface was then ~~of~~ 115 m and decreased to about 36 m at 210 m ~~in~~ depth. The vent subsequently widened to the steady surface diameter of nearly 200 m at the time of our survey in 2015 where the top of the magmatic column was varying between the altitude of the floor of Halemaʻumaʻu crater to nearly 200 m in depth.

### 3.1. Qualitative observations

The main feature of the 3D model (Fig. 3a and b; Supplementary data B) is that the area of Halemaʻumaʻu is globally conductive. This is in agreement with the strong hydrothermal activity observed at the surface. High conductivity values are particularly extensive all around the crater where surface altered areas are collocated with positive self-potential and temperature anomalies (Fig. 3d). In the southern area of Halemaʻumaʻu crater, two main conductive zones can be distinguished (Fig. 3b and Supplementary data B). The one to the southeast (conductor C1 on Fig. 3 a and b) coincides in part with the lava lake, and the second, wider one at the southwest, is clearly related to the hydrothermal system (conductor C2 on Fig. 3 a, b and c). During the collapse of a large part of the caldera, related to the 2018 East Rift Zone eruption, we observed that the hydrothermally altered zones coincided with the major faults of the collapse. The superimposition of the 3D conductivity model at 50 m in depth (conductors C3 and C4 on Fig. 3a) or of the extent of the hydrothermal areas (Fig. 3e) with the extent of the collapsed zone between May 31 and July 8 2018, shows this correlation. This consistency is especially well evidenced to the northeast at the scale of the NE conductor C4 (Fig. 3c). At the beginning, the collapse was focused on

**Fig. 3.** 3D conductivity model of the lava lake and its environment a) at a depth of 50 m below the lava lake surface. RMS 6, 18 iterations. DEM from http://opentopo.sdsc.edu/lidarDataset?opentopoID=OTLAS.032012.32605.1. The radar image (Italian Space Agency's Cosmo-SkyMed satellite system; https://volcanoes.usgs.gov/observatories/hvo/multimedia_uploads/multimediaFile-2556.gif) in right-bottom inset shows enlargement of summit eruptive vent from May 31 and July 8, 2018. The black star locates the VLP source from Dawson et al. (2010) at a depth of about 1 km below the caldera floor. b) SWRZ-lava lake-ERZ slice within the 3D model shown in a, and associated sensitivity. A zoom on the lava lake is framed in red. c) NW-SE and SW-NE slices within the 3D model shown in a. Areas unconstrained in the model are blanked (i.e. sensitivity <−10). 3D topography from Google Earth. d) Qualitative comparison between 3D and 2D models showing the main distribution of the hydrothermal system superimposed to the thermal anomaly map. Main eruptive axis from Neal and Lockwood (2003). e) 2018 crisis main axes of fracturing and subsidence of Halemaʻumaʻu crater and caldera floor on July 8, 2018 (georeferenced from radar images and WorldView-3 satellite; USGS-HVO website) superimposed to the distribution of the hydrothermal system inferred from conductivity model and thermal anomaly map. (For interpretation of the references to colour in this figure legend, the reader is referred to the web version of this article.)

the area of the lava lake and of the VLP source (Dawson and Chouet, 2014) (Fig. 3a). The latter was attributed to the persistent unsteady flow of magma through a complex system of sills and dikes in the shallow plumbing system of Kīlauea (Chouet and Dawson, 2013; Chouet and Matoza, 2013). These observations (i.e., highly conductive zones, seismic activity and collapse focus) demonstrate the connection between the magmatic and hydrothermal systems in this area.

### 3.2. A magma body concealed in its surrounding hydrothermal system

Based on the conductivity distribution and its values, it is not possible to unambiguously identify the presence of a magma column beneath the lava lake, in agreement with our sensitivity testing from forward modelling using theoretical conductivity patterns (Fig. A1 in Supplementary data A). The presence of wide volumes of hydrothermal alteration and hot fluids implies that the medium has a high general conductivity and therefore a limited conductivity contrast with that expected for the magma column. The 3D conductivity distribution model and theoretical resistivity estimates allow us to distinguish four main conductivity regions.

- The area of the lava lake (conductor C1; 0.14 S/m) coincides with a more diffuse and wider conductive zone than expected for the magmatic body alone.
- The hydrothermal system surrounding the magmatic column should have slightly lower conductivity values (conductor C1; ~1.67 $10^{-2}$ S/m) than the magma column. However, the presence of a large amount of gas bubbles in the upper part of the lake may result in decreasing the conductivity contrast between the magma and the hydrothermal system. Furthermore, the magma column itself is a source of heat and fluids for the surrounding medium. In eight years (since 2008), it is conceivable that a crown of enhanced hydrothermal activity and elevated temperature has developed around the magma column, thus increasing the conductivity in a volume larger than that of the column. Rock alteration by volcanic gases is influenced by the properties of the fumarolic gases (Iwasaki et al., 1964). This pattern is particularly important at Kīlauea where gases emitted near the lava lake are very hot (~600 °C) and mostly composed of water, $CO_2$, and $SO_2$. We therefore postulate that the high conductivity anomaly in the area of the lava lake is created by a combined effect of both the magma column and by the surrounding hydrothermal system.
- Away from the magma column of the lava lake, the main conductive areas to the WSW and the patches to the N of Halema'uma'u crater should not be influenced directly by the lava lake, but by deeper sources.
- The conductive zones lie in a water-unsaturated low temperature medium corresponding to the caldera's dense pile of lava flows (resistant R; >1500 Ω.m).

### 3.3. Volcano-tectonic control on the hydrothermal activity

The presence of widespread and strong hydrothermal activity is therefore the main obstacle to clearly differentiate a very high conductivity magma column in this context. The extent of the hydrothermal zones may be refined with the help of the surface thermal anomalies, outcrops of hydrothermal alteration and by the conductivity models.

As it is common in inversion methods, the use of smoothness factors tends to blur the structures at depth and fails to define their depth extent. Accordingly, the conductivity structures have probably more focused boundaries and vertical extent than are shown in the models. On Fig. 3d we have classified the distribution of the hydrothermal system as: (1) highly conductive layer rising to the surface, (2) present at depth or (3) absent. These observations are interpolated with the help of the thermal anomaly map (Patrick and Witzke, 2011) between the profiles. Indeed, it is well established that there is a relationship between surface temperature anomalies and the presence of hydrothermal activity in this context. The sharp and near vertical conductivity contrasts observed on the 2D inversion models of the profiles are also shown on Fig. 3d. These characteristics suggest that volcano-tectonic features such as collapse faults and intrusive fractures may control the extent of hydrothermal zones. As shown on Fig. 3e, the hydrothermally altered zones constitute mechanical heterogeneities and large areas of weakness that influence the development of the collapse faults.

## 4. Discussion and conclusions

Without the presence of a visible magma column, the interpretation of the resistivity measurements at the summit of Kīlauea would remain ambiguous. Unless the magma body was much larger or the surrounding medium was more resistive, it will always be difficult to distinguish magma in this context. The fact that the upper part of the column is highly vesiculated (as demonstrated by the present study on ejected samples: Fig. 2b, and gravity monitoring by Carbone et al., 2013) may explain why this part of the column has a lower conductivity than that obtained on laboratory measurements considering 80% of resistive spherical gas vesicles.

This high vesicularity further contributes to lowering the conductivity contrast between the hydrothermal zone and the magma column.

Based on the observations at the surface and the interpretation of the modelled conductivity distribution, an interpretative scheme has been constructed (Fig. 4). The East Rift Zone eruption of 2018 and the associated summit collapse show that the lava lake was connected to a magma reservoir that was drained during the eruption along the East Rift Zone.

Two types of hydrothermal circulation may be present in the studied zone. The first one is associated ~~to~~ with the collapse faults of Halema'uma'u crater. It explains the high conductivity values in Halema'uma'u and on its rim~~s~~. The magmatic column of the lava lake is emplaced along the eastern rim fault of Halema'uma'u crater, which thus acts as preferential pathway for both hydrothermal circulation and magmatic intrusion. For this reason, the high conductivity values linked to hydrothermal activity and the presence of magma are collocated. This results in the ambiguous identification of the magmatic system within its hydrothermal environment. When the summit vent opened in 2008, one interesting point is that much of the tephra produced in that explosion was heavily coated with anhydrite and natroalunite. Such samples differ greatly from alteration related to hot springs sinter deposits (Bishop, 2011; DeSmither, 2011), implying that the surficial deposits had been heavily altered by sulfuric acid. Accordingly in the lava lake area, the shallow hydrothermal alteration could be driven from deeper processes. Alteration could therefore be more intense around the magmatic conduit than elsewhere, as suggested by our study.

The second, broader, hydrothermal region is located outside of the crater where elongated hydrothermal zones (with the example of anomaly C3 to the north of the crater, Fig. 3a and c) are more likely attributed to larger scale fracturing such as ancient caldera rims (Swanson et al., 2012) and/or to dyke-shaped intrusions. These fractures have created weakness or more permeable areas and therefore preferential hydrothermal and magmatic fluids pathways within the edifice.

The model presented in this study is derived from 3D inversion. We show the importance of considering 3D forward models in order to optimize the 3D survey protocol to image the targeted structures. Additional data and more sophisticated 3D electrical modelling software could also depict a clearer picture of such a magmatic body from conductivity data. It remains that our experience has emphasized the difficulties of unambiguously identifying magma at depth with resistivity measurements. This goes beyond the case of Kīlauea and is an issue in all magmatic systems. In order to address it, more work is necessary in several directions: types of measurements (such as deep 3D ERT,

magnetic measurements as an example), laboratory calibration and model computation using complementary datasets. In the case of extensive hydrothermal alteration, the joint study of several geophysical types of data (conductivity, induced polarization, seismic, magnetic) may help to distinguish high conductivity values associated with hydrothermal activity from those associated with magma bodies.

Magmatic bodies and hydrothermally altered rocks are among the main zones of weakness at various depths and lateral extents in volcanoes. The 2018 crisis and the associated major collapse event ~~that occurs~~ at Kīlauea volcano is a strong example of the large increase of hazards due to surrounding hydrothermal system. However, the geometry and extent of such systems remain difficult to constraint in depth. Here we contribute to image the extent of this hydrothermal system both laterally and in depth, that should, at least in part, have an influence on volcano-tectonic evolution. Combining such high-resolution geophysical surveys interpreted under geological and physical constraints therefore remains one of the most powerful tools for quantifying hazards at many other volcanoes (Finn et al., 2001).

Supplementary data to this article can be found online at https://doi.org/10.1016/j.jvolgeores.2019.06.001.

## Acknowledgements

This study was funded by the Laboratory of Excellence ClerVolc and partly on behalf of a CNRS INSU project. We are grateful to Tina Neal, Jeff Sutton, Don Swanson, Steve Brantley and all the HVO's staff, Philippe Labazuy, Thierry Souriot, Yohan Gardes and the OPGC staff, for their scientific and logistic support, before, during and after the survey. We also thank the Hawai'i Volcanoes National Park for their support, and USGS as information sources. We also warmly acknowledge all the volunteers, Bernadette Lénat, Bernard Contarin, Béatrice Chevallet and Guy Chevallet, for their contribution to this project. Thanks for the technical advices of STRATAGEM974 for the preparation of the ERT field work and data processing. This is Laboratory of Excellence ClerVolc contribution n° 346. Computations presented in this paper were performed using the Froggy platform of the CIMENT infrastructure (https://ciment.ujf-grenoble.fr), which is supported by the Région Auvergne-Rhône-Alpes (grant CPER07_13 CIRA), the OSUG@2020 LABEX (reference ANR10 LABX56), and the Equip@Meso project (reference ANR-10-EQPX-29-01) of the program 'Investissements d'Avenir' supervised by the Agence Nationale de la Recherche. 3D conductivity images were generated thanks to VisIt software. The manuscript greatly benefited from the comments and reviews from Alessandro Aiuppa, Donald Swanson an anonymous reviewer, to whom we offer our thanks.

## References

Bartel, L.C., Hardee, H.C., Jacobson, R.C., 1983. An electrical resistivity measurement in molten basalt during the 1983 Kilauea eruption. Bull. Volcanol. 46, 271–276.
Bishop, R.A., 2011. Mineralogical Study of Volcanic Sublimates From Halema'uma'u Crater, Kilauea Volcano. Hawaii Space Grant Consortium.
Blakely, R.J., 1988. Curie temperature isotherm analysis and tectonic implications of aeromagnetic data from Nevada. J. Geophys. Res. Solid Earth 93, 11817–11832. https://doi.org/10.1029/JB093iB10p11817.
Carbone, D., Poland, M.P., 2012. Gravity fluctuations induced by magma convection at Kīlauea volcano, Hawai'i. Geology 40, 803–806. https://doi.org/10.1130/G33060.1.
Carbone, D., Poland, M.P., Patrick, M.R., Orr, T.R., 2013. Continuous gravity measurements reveal a low-density lava lake at Kīlauea Volcano, Hawai'i. Earth Planet. Sci. Lett. 376, 178–185. https://doi.org/10.1016/j.epsl.2013.06.024.
Chouet, B., Dawson, P., 2013. Very long period conduit oscillations induced by rockfalls at Kilauea Volcano, Hawaii. J. Geophys. Res. Solid Earth 118, 5352–5371. https://doi.org/10.1002/jgrb.50376.
Chouet, B.A., Matoza, R.S., 2013. A multi-decadal view of seismic methods for detecting precursors of magma movement and eruption. J. Volcanol. Geotherm. Res. 252, 108–175. https://doi.org/10.1016/j.jvolgeores.2012.11.013.
Dawson, P., Chouet, B., 2014. Characterization of very-long-period seismicity accompanying summit activity at Kīlauea Volcano, Hawai'i: 2007–2013. J. Volcanol. Geotherm. Res. https://doi.org/10.1016/j.jvolgeores.2014.04.010.
Dawson, P.B., Benítez, M.C., Chouet, B.A., Wilson, D., Okubo, P.G., 2010. Monitoring very-long-period seismicity at KilaueaVolcano, Hawaii. Geophys. Res. Lett. 37. https://doi.org/10.1029/2010GL044418.
DeSmither, L., 2011. Distribution of Opaline Alteration in Fumaroles From Halema'uma'u Crater, Kilauea Volcano. Hawaii Space Grant Consortium.
Eychenne, J., Houghton, B.F., Swanson, D.A., Carey, R.J., Swavely, L., 2015. Dynamics of an open basaltic magma system: the 2008 activity of the Halema'uma'u Overlook vent, Kīlauea Caldera. Earth Planet. Sci. Lett. 409, 49–60. https://doi.org/10.1016/j.epsl.2014.10.045.
Finn, C.A., Sisson, T.W., Deszcz-Pan, M., 2001. Aerogeophysical measurements of collapse-prone hydrothermally altered zones at Mount Rainier volcano. Nature 409, 600–603.
Formenti, Y., Druitt, T., 2003. Vesicle connectivity in pyroclasts and implications for the fluidisation of fountain-collapse pyroclastic flows, Montserrat (West Indies). Earth Planet. Sci. Lett. 214. https://doi.org/10.1016/S0012-821X(03)00386-8.
Gailler, L.-S., Lénat, J.-F., Blakely, R.J., 2016. Depth to Curie temperature or bottom of the magnetic sources in the volcanic zone of la Réunion hot spot. J. Volcanol. Geotherm. Res. 324. https://doi.org/10.1016/j.jvolgeores.2016.06.005.
Gailler, L., Arcay, D., Münch, P., Martelet, G., Thinon, I., Lebrun, J.F., 2017. Forearc structure in the Lesser Antilles inferred from depth to the Curie temperature and thermo-mechanical simulations. Tectonophysics https://doi.org/10.1016/j.tecto.2017.03.014.
Gambino, S., Guglielmino, F., 2008. Ground deformation induced by geothermal processes: a model for La Fossa Crater (Vulcano Island, Italy). J. Geophys. Res. Solid Earth 113. https://doi.org/10.1029/2007JB005016 n/a–n/a.
Holcomb, R.T., 1987. Eruptive history and long-term behavior of Kīlauea volcano, in: Volcanism in Hawaii. US Geol. Surv. Prof. Pap. 1350, 261–350.
Houghton, B.F., Wilson, C.J.N., 1989. A vesicularity index for pyroclastic deposits. Bull. Volcanol. 51, 451–462.
Hurwitz, S., Christiansen, L.B., Hsieh, P.A., 2007. Hydrothermal fluid flow and deformation in large calderas: inferences from numerical simulations. J. Geophys. Res. Solid Earth 112. https://doi.org/10.1029/2006JB004689.
Iwasaki, I., Hirayama, M., Katsura, T., Osawa, T., Ossaka, J., Kamada, M., Matsumoto, H., 1964. Alteration of rock by volcanic gas in Japan. XIII General Assembly. IUGG.
Johnson, T.C., Versteeg, R.J., Ward, A., Day-Lewis, F.D., Revil, A., 2010. Improved hydrogeophysical characterization and monitoring through parallel modeling and inversion of time-domain resistivity and induced-polarization data. Geophysics 75, WA27–WA41. https://doi.org/10.1190/1.3475513.
Lees, J.M., 2007. Seismic tomography of magmatic systems. J. Volcanol. Geotherm. Res. 167, 37–56.
Legaz, A., Vandemeulebrouck, J., Revil, A., Kemna, A., Hurst, A.W., Reeves, R., Papasin, R., 2009. A case study of resistivity and self-potential signatures of hydrothermal instabilities, Inferno Crater Lake, Waimangu, New Zealand. Geophys. Res. Lett. 36, L12306. https://doi.org/10.1029/2009GL037573.
Lénat, J.F., 1995. Geoelectrical methods in volcano monitoring. Monitoring Active Volcanoes: Strategies, Procedures and Techniques. UCL Press, London.
Murase, T., McBirney, A.R., 1973. Properties of some common igneous rocks and their melts at high temperature. Geol. Soc. Am. Bull. 84, 3563–3592.
Neal, C.A., Lockwood, J.P., 2003. Geologic map of the summit region of Kīlauea Volcano, Hawaii: U.S. Geol. Surv. Geol. Investig. Ser. I-2759, scale 124,000, 14 p.
Neal, C.A., Brantley, S.R., Antolik, L., Babb, J.L., Burgess, M., Calles, K., Cappos, M., Chang, J.C., Conway, S., Desmither, L., Dotray, P., Elias, T., Fukunaga, P., Fuke, S., Johanson, I.A., Kamibayashi, K., Kauahikaua, J., Lee, R.L., Pekalib, S., Miklius, A., Million, W., Moniz, C.J., Nadeau, A., Okubo, P., Parcheta, C., Patrick, M.R., Shiro, B., Swanson, D.A., Tollett, W., Trusdell, F., Younger, E.F., Zoeller, M.H., Montgomery-Brown, E.K., Anderson, K.R., Poland, M.P., Ball, J.L., Bard, J., Coombs, M., Dietterich, H.R., Kern, C., Thelen, W.A., Cervelli, P.F., Orr, T., Houghton, B.F., Gansecki, C., Hazlett, R., Lundgren, P., Diefenbach, A.K., Lerner, A.H., Waite, G., Kelly, P., Clor, L., Werner, C., Mulliken, K., Fisher, G., Damby, D., 2019. The 2018 rift eruption and summit collapse of K ī lauea Volcano. Science 363, 367–374.
Ni, H., Keppler, H., Behrens, H., 2011. Electrical conductivity of hydrous basaltic melts: Implications for partial melting in the upper mantle. Contrib. to Mineral. Petrol. 162, 637–650. https://doi.org/10.1007/s00410-011-0617-4.
Orr, T.R., Thelen, W.A., Patrick, M.R., Swanson, D.A., Wilson, D.C., 2013. Explosive eruptions triggered by rockfalls at Kīlauea volcano, Hawai'i. Geology https://doi.org/10.1130/G33564.1.
Patrick, M.R., Witzke, C.N., 2011. Thermal mapping of Hawaiian volcanoes with ASTER satellite data. U. S. Geol. Surv. Sci. Investig. Rep. 2011–5110 (22 pp.).
Patrick, M., Wilson, D., Fee, D., Orr, T., Swanson, D., 2011. Shallow degassing events as a trigger for very-long-period seismicity at Kīlauea Volcano, Hawai'i. Bull. Volcanol. 73, 1179–1186. https://doi.org/10.1007/s00445-011-0475-y.
Patrick, M.R., Orr, T., Lee, L., Moniz, C., 2015. A multipurpose camera system for monitoring Kilauea Volcano, Hawai'I. U.S. Geological Survey Techniques and Methods Book, p. 13.
Patrick, M.R., Orr, T., Sutton, A.J., Lev, L., Thelen, W., Fee, D., 2016. Shallowly driven fluctuations in lava lake outgassing (gas pistoning), Kilauea Volcano. Earth Planet. Sci. Lett. 433, 326–338. https://doi.org/10.1016/j.epsl.2015.10.052.
Peck, D.L., 1978. Cooling and vesiculation of Alae lava lake, Hawaii. U.S. Geol. Surv. Prof. 935B, 59.
Poland, M.P., Carbone, D., 2016. Insights into shallow magmatic processes at Kīlauea Volcano, Hawai'i, from a multiyear continuous gravity time series. Geophys. Res. Solid Earth 121, 5477–5492.
Pommier, A., Le-Trong, E., 2011. "SIGMELTS": a web portal for electrical conductivity calculations in geosciences. Comput. Geosci. 37, 1450–1459.
Powers, H.A., 1948. A chronology of the explosive eruptions of Kilauea. Pacific Sci 2, 278–292.
Pritchard, M.E., Gregg, P.M., 2016. Geophysical Evidence for Silicic Crustal Melt in the Continents: Where, What Kind, and How Much? , pp. 121–128 https://doi.org/10.2113/gselements.12.2.121
Revil, A., Jardani, A., 2010. Seismoelectric response of heavy oil reservoirs: theory and numerical modelling. Geophys. J. Int. 180, 781–797. https://doi.org/10.1111/j.1365-246X.2009.04439.x.

Revil, A., Hermitte, D., Spangenberg, E., Cochemé, J.J., 2002. Electrical properties of zeolitized volcaniclastic materials. J. Geophys. Res. 107, 2168. https://doi.org/10.1029/2001JB000599.

Revil, A., Finizola, A., Sortino, F., Ripepe, M., 2004. Geophysical investigations at Stromboli volcano, Italy: implications for ground water flow and paroxysmal activity. Geophys. J. Int. 157, 426–440.

Revil, A., Finizola, A., et al., 2008. Inner structure of La Fossa di Vulcano (Vulcano Island, southern Tyrrhenian Sea, Italy) revealed by high resolution electric resistivity tomography coupled with self-potential, temperature, and soil CO2 diffuse degassing measurements. J. Geophys. Res. 113, B07207.

Richter, N., Poland, M.P., Lundgren, P.R., 2013. TerraSAR-X interferometry reveals small-scale deformation associated with the summit eruption of Kīlauea Volcano, Hawai'i. Geophys. Res. Lett. 40, 1279–1283. https://doi.org/10.1002/grl.50286.

Roche, O., Druitt, T.H., Merle, O., 2000. Experimental study of caldera formation. J. Geophys. Res. 105, 395–416.

Smith, B.D., Zablocki, C.J., Frischknecht, F., Flanigan, V.J., 1977. Summary of results of electromagnetic and galvanic soundings on Kilauea Iki lava lake, Hawaii. US Geol. Surv. Rep. 77–59.

Swanson, D., Wooten, K., Orr, T., 2009. Buckets of ash track tephra flux from Halema'uma'u crater, Hawai'i. EOS Trans. Am. Geophys. Union 90, 427.

Swanson, D.A., Rose, T.R., Fiske, R.S., McGeehin, J.P., 2012. Keanakāko'i Tephra produced by 300 years of explosive eruptions following collapse of Kīlauea Caldera in about 1500 CE. J. Volcanol. Geotherm. Res. 215–216, 8–25. https://doi.org/10.1016/j.jvolgeores.2011.11.009.

Swanson, D.A., Rose, T.R., Mucek, A.E., Garcia, M.O., Fiske, R.S., Mastin, L.G., 2014. Cycles of explosive and effusive eruptions at Kīlauea Volcano, Hawai'i. Geology 2 (42), 631–634. https://doi.org/10.1130/G35701.1 (IP-055751).

Tanaka, A., Okubo, Y., Matsubayashi, O., 1999. Curie point depth based on spectrum analysis of the magnetic anomaly data in East and Southeast Asia. Tectonophysics 306, 461–470. https://doi.org/10.1016/S0040-1951(99)00072-4.